# Effects of mobile charged defects on current–voltage behavior in resistive switching memories based on organic–inorganic hybrid perovskite

Arijit Roy,[1] Ho Won Jang,[2] and Pil-Ryung Cha[1,a)]

[1]School of Materials Science and Engineering, Kookmin University, Seoul 02707, South Korea
[2]Department of Materials Science and Engineering, Seoul National University, Seoul 08826, South Korea

*I–V* characteristics that are commonly observed in resistive switching memories based on organic or organic–inorganic hybrid materials are investigated using a drift–diffusion model. The characteristic current deflection region at a specific voltage in a high-resistance-state (HRS) is predicted using the drift-diffusion model and compared with the experimental results of methylammonium lead iodide (MALI, $CH_3NH_3PbI_3$). The accumulation of oppositely charged defects in the Debye layers is found to play a dominant role in determining the shape of the *I–V* curve in the HRS. The magnitude of the applied voltage at which the deflection in the current occurred is decreased by increasing the voltage sweep rate. This result is attributed to the time-dependent migration of charged defects from the Debye layers to the bulk of the switching materials. *Published by AIP Publishing.* https://doi.org/10.1063/1.5051499

The development of new-generation perovskite insulating materials for resistive memory devices gains much attention in recent years. Organic–inorganic hybrid perovskites such as MALI ($CH_3NH_3PbI_3$), as strong candidates for next-generation solar cell materials, have been reported to exhibit resistive memory characteristics. MALI has become a subject of interest as a next-generation memristor material.[1,2] Other organic–inorganic hybrid perovskites having different halide elements, such as $CH_3NH_3PbBr_3$[3] quantum-dot perovskites, or mixed halides, such as $CH_3NH_3PbI_{3-x}$ $Cl_x$,[4,5] $CH_3NH_3PbBr_{3-x}$ $Cl_x$,[6] and $CH_3NH_3PbI_{3-x}$ $Br_x$,[7] are also promising as candidate materials for memristor applications. Many inorganic perovskites, including $CsPbBr_3$,[8] $Pr_{0.7}Ca_{0.3}MnO_3$,[9] and Cr-doped $SrTiO_3$,[10] have also been explored as potential memristor materials. Despite the interest and versatility in the choice of materials, considerable numerical investigations on the role of charged point defects transport—such as defects with negative charge; halide interstitials, metal vacancies, and vacancies of organic moieties, as well as defects with positive charge; halide vacancies, metal interstitials, and interstitials of organic moieties[11]—to correlate the observed *I–V* behaviour are still required. Numerical studies to explore the role of charged defect migration in oxide memristors[12–16] can be mentioned.

In hybrid perovskites with single as well as mixed halide contributions, positively charged halide vacancies such as I and Br vacancies are relatively mobile as compared with other charged species due to a low activation barrier.[7,17] For example, the diffusion coefficient of the I vacancy in MALI is of the order of $10^{-16} m^2/s$.[18] Point defects having this magnitude of diffusion coefficient can travel considerable distances in the perovskite memristor at the time scale on which the *I–V* measurement is performed, resulting in changes in the internal electric field and subsequently affecting the *I–V* curve measurement. Therefore, these defects are closely related to the observed switching characteristics. On the other hand, in the case of $CsPbBr_3$, migration of Br ions

was proposed to be responsible for the possible switching mechanism.[8] In the case of $Pr_{0.7}Ca_{0.3}MnO_3$ and Cr-doped $SrTiO_3$, the movement of charged defects under the applied electric field such as oxygen ions[9] and oxygen vacancies[10] plays an important role in resistive switching. We are interested in exploring the role of these charged defects during the operation condition of the memristor. For this purpose, we choose MALI as a candidate material. Our study can be extended to other memory switching materials as well.

The mechanism by which diffusion of charged point defects affects the internal electric field distribution is as follows: when a voltage is applied to both sides of a resistive switching layer, the internal point defects move to the electrodes according to their charge polarities. The point defects that move to the electrodes form a nanometer-scale electric double layer (EDL) in front of them. This EDL is called the Debye layer. For example, the thickness of the Debye layer for MALI is about 1.5 nm.[19] The point defects accumulated in the Debye layer effectively cut off the voltage between the electrodes, thereby drastically reducing the strength of the internal electric field.[20] The driving force for the diffusion of the charged species also reduces due to the drop in the internal electric field. This affects the measurement of current and thereby the state of resistance in the memristor.

In the case of resistive switching memories, distinguishable resistance states are observed. In particular, when a perovskite memristor is subjected to a positive sweeping voltage, resistance changes from a high to a low value at a critical applied voltage and the measured current increases in the process. The state of resistance which has increased measured current is known as the low-resistance-state or LRS. On the other hand, current decreases abruptly at a specific applied voltage during the application of negative sweeping voltage; the state of resistance having decreased measured current is known as the high-resistance-state or the HRS. Different conduction mechanisms are employed to explain the typical *I–V* characteristic observed in HRS and LRS. As investigated by Gu and Lee,[2] Ohmic and space-charge-

limited conduction (SCLC) mechanisms play the key role. At a low applied voltage, thermally generated defects are more dominant compared with defects generated by the applied electric field. Thus, the trap states are partially filled and Ohmic conduction is observed. On the other hand, at a high applied voltage, the charged defects become more dominant and SCLC behavior in the $I$–$V$ curve is observed. However, Park $et$ $al.$[21] found that the thermal-hopping assisted charge transfer between different trap states are more relevant explanation of the high voltage $I$–$V$ behavior. During the application of the positive and negative voltage sweeps, the applied electric field can be fully compensated by the defect generated electric field—due to the accumulation of oppositely charged defects in EDL. The electric field originating from the defects may also be referred to as the nano-battery effect.[22–24] Because of the absence of driving force, measured electric current becomes zero. In typical $I$–$V$ curves (logarithm of absolute current versus voltage), the reduction in current at the HRS results in current deflection regions. It is found that retention and endurance of resistive switching devices are strongly influenced by the drop in the electric field (nano-battery effect),[23] resulting in a region of current deflection points in $I$–$V$ curves. Hence, it is important to explore its effect from the application point of view.

We follow the simulation methodology proposed by Foster $et$ $al.$[25] and Richardson $et$ $al.$[20] to model the diffusion of charged point defects due to the defect concentration gradient and electric field. This model was originally applied to $I$–$V$ behavior analyses of MALI solar cells. To obtain the similar $I$–$V$ behaviour in the case of memristor, a voltage is applied in the system at different sweeping rates. The internal distribution of electric potential ($\Phi$) and therefore the generated electric field, $E_{bulk}(t)$, can be calculated by solving the Poisson's equation of charge conservation. We consider only one predominant charged defect—positively charged halide vacancy.[18,26] In contrast to the modelling approach considered for solar cells, the concentration of the hole is not necessary in the memristor application. Therefore, we neglected this contribution in our simulation. The spatial and temporal distribution of the concentration for the halide vacancy and the electron can be calculated from the following diffusional flux:

$$J_v = D_V[\nabla C_V - C_V/(k_B T)\,\nabla\Phi],\qquad(1)$$

$$J_e = D_e[\nabla n_e - n_e/V_T\,E_{bulk}].\qquad(2)$$

Here, $J_v$ is the vacancy flux and $J_e$ is the flux for the electron. The concentrations for the vacancy and the electron are written as $C_V$ and $n_e$, respectively. $D_v$ and $D_e$ are the diffusivities of the vacancy and the electron, respectively.

We can reproduce the $I$–$V$ curve of the perovskite by solving the equations for $E_{bulk}$, $C_V$, and $n_e$. However, it is practically impossible to simulate the $I$–$V$ curve in the experimental time scale by simultaneously solving these equations numerically. The reasons are as follows. First, the diffusivity of the halide vacancy[19] and that of the electron[27] are (in general) about 12 orders of magnitude different. Second, the thickness of the Debye layer is about 1.5 nm. Therefore, a grid that is much smaller than 1.5 nm in size should be used.

To solve the problem numerically, the following approximation method used in a previous Ref. 20 is adopted for this study. The halide vacancy has a positive charge and accumulates in the Debye layer when the electric field is applied, causing a voltage drop. To rigorously describe this behavior, we need to solve the equation for the vacancy concentration in time and space. However, since the diffusivity of the halide vacancy is $\approx 10^{-16}$ m$^2$/s, the numerical simulation using the explicit Euler method cannot describe the time scale of the experimentally measured $I$–$V$ curves, because the limitation on the temporal step size becomes too severe. To solve this problem, instead of solving the equation for the vacancy concentration, the concentration of halide vacancy accumulated in the Debye layer is approximated as follows:[25]

$$\frac{dC_V}{dt} = \frac{qD_V N_V^{eq}}{V_T}E_{bulk}(t).\qquad(3)$$

The electric charge accumulated in the Debye layer from Eq. (3) can be approximated by $Q_+ = qC_V$. Due to the charge neutrality condition, the charge accumulated on the opposite electrode becomes $Q_- = -Q_+$.

The following asymptotic approximation solution was used for the mobile charge that is accumulated in the Debye layer to overcome the limitation on the grid size due to the thickness of the Debye layer:[20,25]

$$Q_{+/-}(V_{+/-}) = \epsilon V_T/L_D \mathbf{sign}(V_{+/-})$$
$$\times \left[2\left(e^{V_{+/-}/V_T} - 1 - V_{+/-}/V_T\right)\right]^{1/2}.\quad(4)$$

The dielectric constant and Debye length of the system are denoted by $\epsilon$ and $L_D$, respectively. Voltage drops $V_+$ and $V_-$ in the Debye layers are yielded by substituting $Q_+$ and $Q_-$ obtained from Eq. (3) into Eq. (4).

Voltage reductions occur in the Debye layers near both electrodes when a voltage is applied. The voltage change inside the bulk can be assumed to be linear. Based on this assumption, the electric field inside the bulk can be approximated as follows:

$$E_{bulk}(t) = (V_{bi} - V(t) - V_+ + V_-)/d,\qquad(5)$$

where $V_{bi}$ is the built-in voltage, $V(t)$ is the external voltage, and $d$ is thickness of the resistive film.

Our simulation methodology can be applied to study the dynamics of charged species due to the applied electric field and thereby the $I$–$V$ behavior for the perovskite memristor. In this study, we choose metal/MALI/metal as the candidate system. The equilibrium iodine vacancy concentration is assumed to be $N_V^{eq} = 1.0 \times 10^{25}$ m$^{-3}$ (Ref. 19). The diffusivities for the vacancy and the electron are considered to be $D_V = 9.5 \times 10^{-16}$ m$^2$/s and $D_e = 1.7 \times 10^{-4}$ m$^2$/s (Ref. 27), respectively. Compared with the study by Eames $et$ $al.$[18] ($1.0 \times 10^{-16}$ m$^2$/s), a slightly large value of $D_V$ is chosen in our simulations to compare our findings with the experimental observation. The absolute temperature and corresponding thermal voltage are set as $T = 298$ K and $V_T = 0.0257$ V, respectively. $\epsilon$ is set to 24.1 $\epsilon_0$.[28] $\epsilon_0$ is the vacuum permittivity. In the simulation, the thickness ($d$) of the MALI film is set as 300 nm and $V_{bi}$ is set to 0 V. To solve the electron
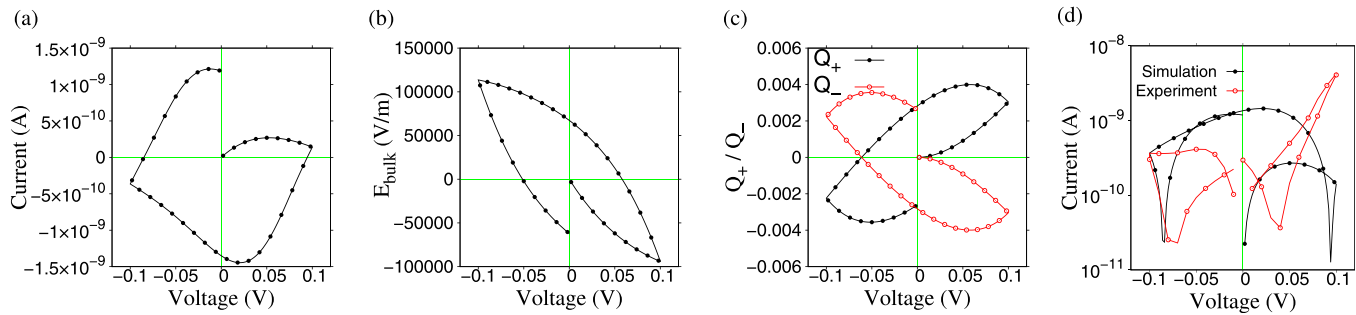
FIG. 1. (a) Current versus voltage hysteresis curve during a voltage sweeping rate of 0.1 V/s. Variation of (b) electric field ($E_{bulk}$) and (c) accumulated charge defect ($Q_+/Q_-$) with applied voltage. (d) Simulated $I$–$V$ curve obtained from the hysteresis plot (a) by considering the logarithm of absolute current and the experimentally obtained $I$–$V$ curve for Pt/MALI/Ag. Experimental data plot (drawn as a red line with open circles) in (d) is Reproduced with permission from Choi *et al*. Adv. Mater. **28**, 6562 (2016).[1] Copyright 2016 John Wiley and Sons.

diffusion equation, we fix the boundary concentration to $n_0^{eq} \exp(-(E_b + V_{+/-})/V_T)$. The concentration value of the free electron in the metal, $n_0^{eq} = 5.8 \times 10^{28}$ m$^{-3}$, and the value for the energy barrier, $E_b = 0.79$ eV, are chosen in such a way that the measured current value is comparable with the experimentally observed $I$–$V$ curve, as shown in Fig. 1(d).

Our study explores the unique behavior of the $I$–$V$ curves in the HRS. We do not consider the switching characteristic, such as set/reset. This is due to the fact that during set/reset operation, a sudden increase/decrease in the current value is typically observed because of the completion/dissolution of the conducting filaments. The motion of ionic species (due to the applied and accumulated charge defect generated electric field) is considered to generate the electric current. However, morphological changes inside the system are not considered. Therefore, the effect of the formation or dissolution of the conducting filaments on the $I$–$V$ behavior is not of concern in this study.

The hysteresis in the measured current value due to applied voltage is shown in Fig. 1(a). The voltage is changed on the order of $0 \rightarrow 0.1 \rightarrow 0 \rightarrow -0.1 \rightarrow 0$ V at a sweeping rate of 0.1 V/s. The typical hysteresis in the measured current value, which is observed in metal/MALI/metal systems, is the characteristics of bi-polar switching. Two points in the curve where the current value becomes zero at a specific applied voltage are observed from our simulations. These points are of particular interest because the electric field inside MALI at these voltages becomes fully compensated by the oppositely charged species that accumulate at the Debye layer near the metallic contacts. Also, the sign of the measured current changes at these voltages. Two regions where the current changes its sign are found during the 0.1 $\rightarrow$ 0 V voltage scan and during the $-0.1 \rightarrow 0$ V voltage scan. This result can be attributed to the change in the polarity of $E_{bulk}$. The variation of $E_{bulk}$ with the applied voltage is observed in Fig. 1(b). As expected, the electric field at specific applied voltages becomes zero during the positive and negative voltage sweeps and its polarity change in the process. Determined from the variations of accumulated opposite charge defects ($Q_+$ and $Q_-$) in the Debye layers as shown in Fig. 1(c), the magnitudes of $Q_+$ and $Q_-$ reach their maximum value during the 0.1 $\rightarrow$ 0 V voltage sweep. $V_+$ and $V_-$ become dominant at this strength of accumulated charge and the applied electric field [$V(t)$] becomes fully

compensated. We can also describe the reason for the compensation of $V(t)$ using similar argument, which leads to the observed zero value of $E_{bulk}$ during the negative voltage sweep. The schematic illustration of the compensation of $E_{bulk}$ during positive and negative voltage sweeps is shown in Fig. 2. It is interesting to observe the discontinuity in the $I$–$V$ and $E_{bulk}$–$V$ curves at 0 V at the end of the negative voltage sweep ($-0.1 \rightarrow 0$ V sweep) in Figs. 1(a) and 1(b), respectively. This is attributed to the finite amount of oppositely charged species ($Q_+$ and $Q_-$) accumulated in the Debye layers at 0 V at the end of $-0.1 \rightarrow 0$ V voltage sweep [as can be seen in Fig. 1(c)].

In typical experimental observations of memresitive devices (if switching occurs), the current becomes negative in the negative voltage sweep. However, in our simulation, the current becomes negative during the 0.1 V $\rightarrow$ 0 V voltage change as shown in Fig. 1(a). This result can be attributed to the formation and dissolution of the conducting filaments during the switching operation. The conducting filaments form during the positive voltage sweep and effectively short circuit the two opposite electrodes. On the other hand, dissolution of conducting filaments starts when negative voltage is applied to the top electrode. Such dissolution in turn generates a negative current value during the 0 $\rightarrow$ $-0.1$ V
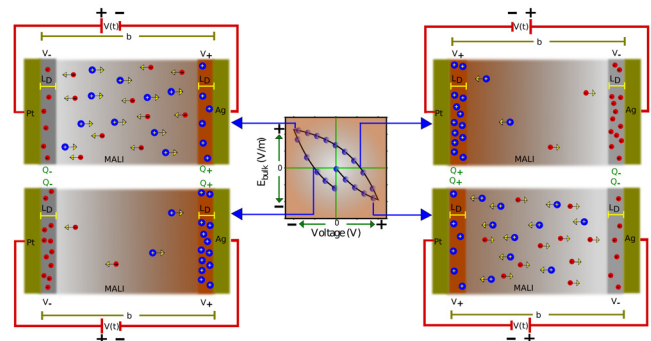


FIG. 2. Schematic illustration of observed $E_{bulk}(t)$ with applied voltage $V(t)$. Different steps of accumulation of charged defects and the formation of Debye layers effecting the measured $E_{bulk}(t)$ are shown. The complete compensation of $E_{bulk}(t)$ (i.e., $E_{bulk}(t) = 0$, which corresponds to zero driving force, leading to zero measured current value—the reason why the current deflection region occurs) is due to the voltage drops $V_+$ and $V_-$ in the Debye layers originating from the accumulated $Q_+$ and $Q_-$ charge are shown in the illustration. Arrows indicate the drifting direction of the charged defects (blue circles with "+" sign) and electrons (red circles with "_" sign).

voltage sweep. Because the morphological changes are not considered in this study, the voltage drop in our simulation due to the Debye layers is dominant in the absence of short-circuit current. During the application of the $0.1 \rightarrow 0\,V$ sweep, the magnitude of the effective electric field is reduced [which can also be seen in Fig. 1(b)] till a specific applied voltage. This reduces the measured current, which finally becomes negative.

Logarithm of the absolute current value is considered and plotted against the applied voltage. The resulting I–V curve is shown in Fig. 1(d) along with the experimentally obtained I–V curve for MALI. The points at which the current become zero during hysteresis lead to the deflection region in the current. As discussed in the previous paragraph, if switching characteristics are observed during the experimental condition, the current deflection region should occur during the negative voltage sweep. However, the voltage in our experimental setup is varied in such a way that the switching does not occur. Therefore, as explained from the simulation results, we can find the current deflection region during the positive voltage sweep in such experimental conditions as well. The details of the MALI sample preparation and experimental conditions are discussed in the supplementary material section. One important aspect to notice here is the fact that two deflection points in the I–V curve, which are formed during the positive and negative voltage sweep, are not observed at the same magnitude of the applied voltage. This suggests that the sweeping of voltages from $0.1\,V \rightarrow 0\,V$ and $_0.1\,V \rightarrow 0\,V$ affects the accumulation of the opposite charge species in the Debye layers.

The effect of the voltage sweep rate in the formation of the current deflection region is explored in Fig. 3. Five different voltage sweep rates are considered here, including 0.2, 0.4, 0.6, 1.0, and 10.0 V/s. The voltage at which the current drop is observed is changed with the sweeping rate. In particular, during the negative voltage sweep, the voltage magnitude at which the current deflection is observed is decreased by increasing the sweeping rate. This result suggests that the time-dependent motion of the accumulated charge near the electrodes plays an important role. During the negative voltage sweep, the accumulated charge defects at a low sweeping rate get more time to move to the bulk of the material than those at a high sweeping rate, because the migration of defects is also limited by ionic mobility. The defect
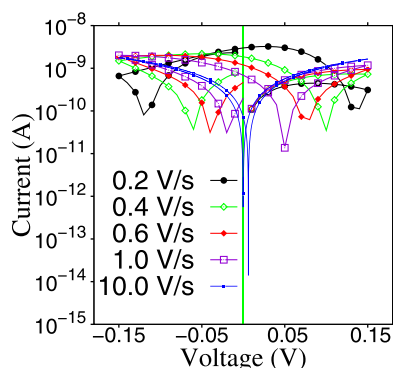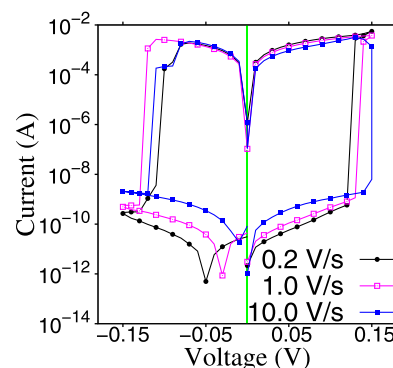


FIG. 4. Experimental I–V curves of Pt/MALI/Ag measured with different voltage sweeping rates. Reproduced with permission from Choi et al. Adv. Mater. 28, 6562 (2016).[1] Copyright 2016 John Wiley and Sons.

generated electric field becomes dominant due to the increasing sweeping rate, which in turn compensates for the applied electric field at a relatively low voltage during the voltage sweeping at a high rate. As shown in Fig. 4, the decrease in the magnitude of voltage at which the deflection in the current occurs during the HRS is also observed in the experimental I–V curve (reproduced from Ref. 1). As seen from the experimental observation, the voltage at which the measured current deflects is decreased by the increasing rate of sweeping. This result facilitates the qualitative validation of our numerical observation with the experiment.

We explore the origin of hysteresis and the typical I–V behavior in the case of resistive memory devices using the drift–diffusion model. We find that the accumulated defects in the Debye layer are the source of the current deflection region that is typically observed in the I–V characteristic in HRS. Moreover, the time-dependent motion of the accumulated defects in the Debye layer affects the formation of the current deflection region. From our simulation, we observe that this deflection shifts toward zero voltage by increasing the sweeping rate. We compare our findings with the experimental observation for the Pt/MALI/Ag memristor. In our simulation, the definition of metal–MALI junctions is very basic, and the properties for these junctions are chosen in terms of model parameters. It is possible to consider the different types of barrier junctions and corresponding free electron densities as per the metal species. However, these choices are beyond the scope of the present study. We believe that this study is helpful in understanding the role of the defect accumulation and in refining operation parameters for resistive memory devices as well.

See supplementary material for material preparation, metal–insulator–metal cell fabrication, and device characterization.

FIG. 3. I–V curves of MALI measured at voltage sweeping rates of 0.2, 0.4, 0.6, 1.0, and 10.0 V/s.

[1]J. Choi, S. Park, J. Lee, K. Hong, D.-H. Kim, C. W. Moon, G. D. Park, J. Suh, J. Hwang, S. Y. Kim, H. S. Jung, N.-G. Park, S. Han, K. T. Nam, and H. W. Jang, Adv. Mater. **28**, 6562 (2016).

[2]C. Gu and J.-S. Lee, ACS Nano **10**, 5413 (2016).

[3]K. Yang, F. Li, C. P. Veeramalai, and T. Guo, Appl. Phys. Lett. **110**, 083102 (2017).

[4]E. J. Yoo, M. Lyu, J.-H. Yun, C. J. Kang, Y. J. Choi, and L. Wang, Adv. Mater. **27**, 6170 (2015).

[5]E. Yoo, M. Lyu, J. H. Yun, C. Kang, Y. Choi, and L. Wang, J. Mater. Chem. C **4**, 7824 (2016).

[6]C. Muthu, S. Agarwal, A. Vijayan, P. Hazra, K. B. Jinesh, and V. C. Nair, Adv. Mater. Interfaces **3**, 1600092 (2016).

[7]B. Hwang, C. Gu, D. Lee, and J.-S. Lee, Sci. Rep. **7**, 43794 (2017).

[8]D. Liu, Q. Lin, Z. Zang, M. Wang, P. Wangyang, X. Tang, M. Zhou, and W. Hu, ACS Appl. Mater. Interfaces **9**, 6171 (2017).

[9]W. Lee, G. Jo, S. Lee, J. Park, M. Jo, J. Lee, S. Jung, S. Kim, J. Shin, S. Park, T. Lee, and H. Hwang, Appl. Phys. Lett. **98**, 032105 (2011).

[10]M. Janousch, G. I. Meijer, U. Staub, B. Delley, S. E. Karg, and B. P. Andreasson, Adv. Mater. **19**, 2232 (2007).

[11]J. Beilsten-Edmands, G. E. Eperon, R. D. Johnson, H. J. Snaith, and P. G. Radaelli, Appl. Phys. Lett. **106**, 173502 (2015).

[12]S. Yu and H. S. Wong, IEEE Electron Device. Lett. **31**, 1455 (2010).

[13]S. Larentis, C. Cagli, F. Nardi, and D. Ielmini, Microelectron. Eng. **88**, 1119 (2011).

[14]F. Nardi, S. Balatti, S. Larentis, and D. Ielmini, *Technical Digest - International Electron Devices Meeting* (IEDM, 2011), p. 709.

[15]S. Kim, S. Choi, and W. Lu, ACS Nano **8**, 2369 (2014).

[16]S. Dirkmann, M. Hansen, M. Ziegler, H. Kohlstedt, and T. Mussenbrock, Sci. Rep. **6**, 35686 (2016).

[17]S. Meloni, T. Moehl, W. Tress, M. Franckevičius, M. Saliba, Y. H. Lee, P. Gao, M. K. Nazeeruddin, S. M. Zakeeruddin, U. Rothlisberger, and M. Graetzel, Nat. Commun. **7**, 10334 (2016).

[18]C. Eames, J. M. Frost, P. R. F. Barnes, B. C. O. Regan, A. Walsh, and M. S. Islam, Nat. Commun. **6**, 7497 (2015).

[19]A. Walsh, D. O. Scanlon, S. Chen, X. G. Gong, and S.-H. Wei, Angew. Chem., Int. Ed. **54**, 1791 (2015).

[20]G. Richardson, S. O'Kane, R. Niemann, T. Peltola, J. Foster, P. Cameron, and A. Walker, Energy Environ. Sci. **9**, 1476 (2016).

[21]N. Park, Y. Kwon, J. Choi, H. W. Jang, P.-R. Cha, N. Park, Y. Kwon, J. Choi, and H. W. Jang, AIP Adv. **8**, 045205 (2018).

[22]I. Valov, E. Linn, S. Tappertzhofen, S. Schmelzer, J. Van Den Hurk, F. Lentz, and R. Waser, Nat. Commun. **4**, 1771 (2013).

[23]S. Tappertzhofen, E. Linn, U. Bottger, R. Waser, and I. Valov, IEEE Electron Device Lett. **35**, 208 (2014).

[24]X. Zhu, J. Lee, and W. D. Lu, Adv. Mater. **29**, 1700527 (2017).

[25]J. M. Foster, H. J. Snaith, T. Leijtens, and G. Richardson, SIAM J. Appl. Math. **74**, 1935 (2014).

[26]T.-Y. Yang, G. Gregori, N. Pellet, M. Grätzel, and J. Maier, Angew. Chem., Int. Ed. **54**, 7905 (2015).

[27]A. Pockett, G. E. Eperon, T. Peltola, H. J. Snaith, A. Walker, L. M. Peter, and P. J. Cameron, J. Phys. Chem. C **119**, 3456 (2015).

[28]F. Brivio, K. T. Butler, A. Walsh, and M. van Schilfgaarde, Phys. Rev. B: Condens. Matter Mater. Phys. **89**, 155204 (2014).